K. Meijer, D. Dudek, A. Ahn, T. Kubow and J. Hearst for comments on earlier drafts, E. Florance for electron microscopy, the University of California Museum of Paleontology electron microscope laboratory and the Scientific Visualization Center at Berkeley.

Correspondence and requests for materials should be addressed to R.J.F. (e-mail: rjfull@socrates.berkeley.edu).

Neural synchrony correlates with surface segregation rules

Miguel Castelo-Branco, Rainer Goebel, Sergio Neuenschwander & Wolf Singer

Max-Planck-Institut für Hirnforschung, Deutschordenstraße 46, 60528 - Frankfurt am Main, Germany

To analyse an image, the visual system must decompose the scene into its relevant parts. Identifying distinct surfaces is a basic operation in such analysis, and is believed to precede object recognition[1,2]. Two superimposed gratings moving in different directions (plaid stimuli) may be perceived either as two surfaces, one being transparent and sliding on top of the other (component motion) or as a single pattern whose direction of motion is intermediate to the component vectors (pattern motion)[3–6]. The degree of transparency, and hence the perception, can be manipulated by changing only the luminance of the grating intersections[7–12]. Here we show that neurons in two visual cortical areas—A18 and PMLS—synchronize their discharges when responding to contours of the same surface but not when responding to contours belonging to different surfaces. The amplitudes of responses correspond to previously described rate predictions[3,13–16] for component and pattern motion, but, in contrast to synchrony, failed to reflect the transition from component to pattern motion induced by manipulating the degree of transparency. Thus, dynamic changes in synchronization could encode, in a context-dependent way, relations among simultaneous responses to spatially superimposed contours and thereby bias their association with distinct surfaces.

Specialized visual neurons may signal the motion of either the individual gratings of a plaid (component-selective cells) or of the global pattern (pattern-selective cells). For the identification of these cells, responses evoked by single gratings were compared to those evoked by unambiguous plaid patterns moving in an intermediate direction, and the results indicate that both cell types exist[3,13–16]. However, except for a single study in the motion sensitive area (MT)of monkey visual cortex[11], no attempt has been made to investigate changes in response amplitudes associated with gradual modifications of transparency conditions. Therefore, little is known about how well individual cells differentiate between component and pattern motion.

Here, we investigate this question with multi-electrode recordings from neurons located in areas A18 and PMLS (postero-medial bank of the lateral suprasylvian sulcus) of the cat visual cortex. In addition, we use cross-correlation analysis to examine the hypothesis that binding of the moving contours into one coherent pattern or two independently moving gratings is associated with changes in the synchronization of responses.

Neurons synchronize their discharges with a precision in the millisecond range if they are activated by single contours, but they do not synchronize when activated by contours of different objects[17–20]. It has been proposed, therefore, that synchronization serves as a binding mechanism by virtue of selectively raising the saliency of the synchronized discharges and thereby favouring their joint processing at subsequent levels. Accordingly, when exposed to plaid stimuli, cells responding to contours of the same surface should synchronize their responses, and cells activated by contours belonging to different surfaces should not synchronize. Which cells are associated with a particular surface depends on transparency conditions, on the match of the cells' preferred direction of motion with the direction of motion of the plaid components and on the spatial relation (overlap, colinearity) of the receptive fields (RFs). In pattern motion, all cells capable of responding to the respective component motions should synchronize their responses because they are excited by contours of the same surface. In component motion, only those cells that respond to the contours of the same component grating should synchronize. This synchronization

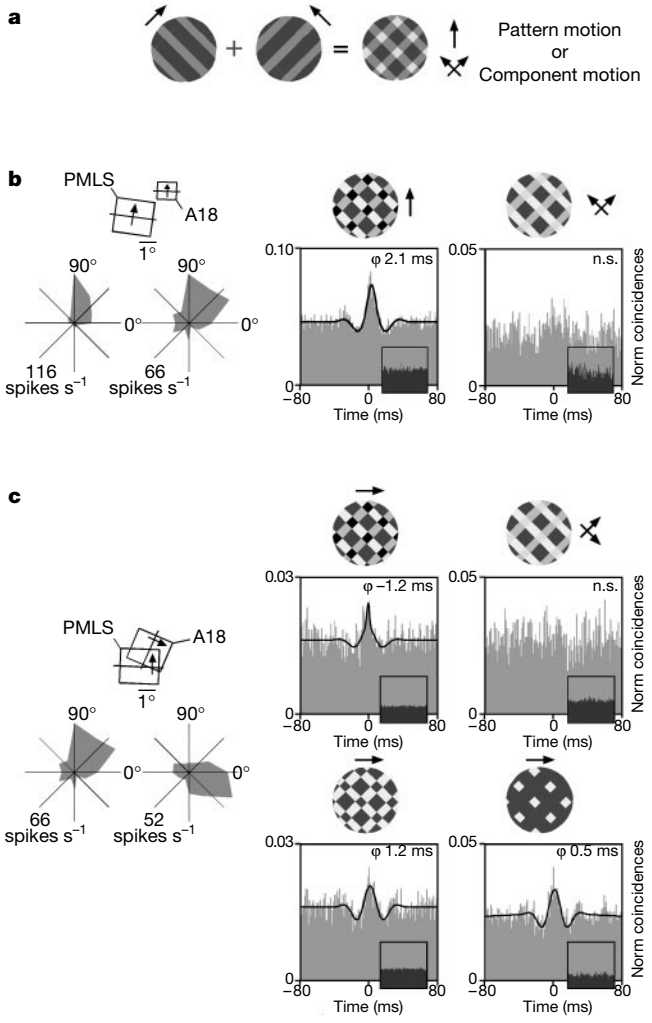

Figure 1 Dependence of synchrony on transparency conditions and receptive field (RF) configuration. **a**, Stimulus configuration. **b**, Synchronization between neurons with non-overlapping RFs and similar directional preferences recorded from A18 and PMLS. Left, RF constellation and tuning curves; right, cross-correlograms for responses to a non-transparent (left) and transparent plaid (right) moving in the cells' preferred direction. Grating luminance was asymmetric to enhance perceptual transparency[3]. Small dark correlograms are shift predictors. **c**, Synchronization between neurons with different direction preferences recorded from A18 (polar and RF plots, left). Top, correlograms of responses evoked by a non-transparent (left) and a transparent (right) plaid moving in a direction intermediate to the cells' preferences. Bottom, correlograms of responses evoked by a non-transparent plaid with reversed contrast conditions (left), and by a surface defined by coherent motion of intersections (right). Scale on polar plots: discharge rate in spikes per second. Scale on correlograms: abscissa, shift interval in ms, bin width 1 ms; ordinate, number of coincidences per trial, normalized. Thick line, fitted gabor function; φ, phase shift. n.s., not significant.

should be particularly robust for cells with colinearly aligned, overlapping RFs as these respond to the same bar of a component grating.

Results of experiments addressing these predictions for cell pairs with different RF configurations are shown in Figs 1–3. Population data are presented in Fig. 4. Figure 1b shows neurons with non-overlapping and non-colinear RFs that have similar direction preference and were recorded simultaneously from areas A18 and PMLS. These cells synchronized in response to non-transparent patterns moving in the neurons' preferred direction but not when activated by a transparent plaid. Figure 1c (top) shows A18 neurons with non-overlapping RFs and different direction preferences. These cells too synchronized in the non-transparent condition when the direction of pattern motion was intermediate between the cells' preferred directions but not in the transparent condition. The synchronization in the non-transparent condition was of similar magnitude for all contrast conditions that bias perception towards pattern motion (Fig. 1c, compare top and bottom).

Figure 2 shows cells recorded from PMLS that had similar direction preferences and colinearly aligned overlapping RFs. These cells synchronized when activated with a single grating moving in their preferred direction and they continued to discharge in synchrony when another grating of different orientation and direction of motion was superimposed, even when transparency conditions were optimal for component motion. This indicates, as predicted, that the responses at both sites had remained associated with contours of the same surface.

To determine whether the degree of synchrony observed with plaids can be accounted for by linear summation of the synchrony induced by each grating alone, we calculated a linear predictor from the sum of coincidences evoked by each grating alone. For neuron pairs with colinear, overlapping RFs (Fig. 2a), synchrony to plaids did indeed correspond to the linear predictor. This was not so for cells with more discordant RFs and differing direction preferences (Fig. 2b). Their responses exhibited strong synchrony when evoked with one of the two gratings but this synchrony broke down when a second transparent grating was superimposed, indicating that addition of the second grating caused active desynchronization. As predicted, cells at the two sites now respond independently to contours of different surfaces.

To exclude the possibility that the changes in synchronization induced by modifications of transparency were due to local contrast changes at the grating intersections rather than to global segmentation processes, we induced the transition from pattern to component motion by changing the ratio (duty cycle) between the width of white and dark bars of the gratings[1,9] (Fig. 3, top). In this case, a gradual change in stimulus parameters leads to an abrupt change in figure–ground assignment. Non-transparent grating intersections suddenly change to background (figure–ground reversal) and this is associated with a sudden switch in perception from pattern to component motion[1,9]. These modifications in duty cycle induce exactly the same changes in synchrony as modifications of transparency conditions by contrast manipulation of intersections (Fig. 3). The relations between synchronization strength, the transparency condition, the direction of plaid motion and the direction preferences of the neuron pairs conform to the predictions (Fig. 3b and c). Cells with differing direction preferences synchronize maximally with non-transparent patterns moving in directions intermediate to the respective preferred directions, but synchrony breaks down when the plaid becomes transparent (Fig. 3b). Some residual synchrony remains when the plaid moves in the opposite direction. In this case synchrony changes only little with transparency, indicating that now both sites respond mainly to contours of one grating. By contrast, synchrony among cells with overlapping, colinearly aligned RFs remains unaffected by changes in transparency. Synchrony varies with the direction of plaid movement but similarly for transparent and non-transparent plaids (Fig. 3c). This agrees with prediction as responses of cells with colinear RFs always remain associated with a single contour that may be either part of a pattern, or one of the two component gratings.

The perceptual switch between component and pattern motion is abrupt. To determine whether this is also the case for synchronization we measured correlation strength with a sliding window analysis while introducing gradual changes of duty cycle. For cells with different direction preference, synchronization broke down abruptly when the pattern became transparent. Correlation peaks

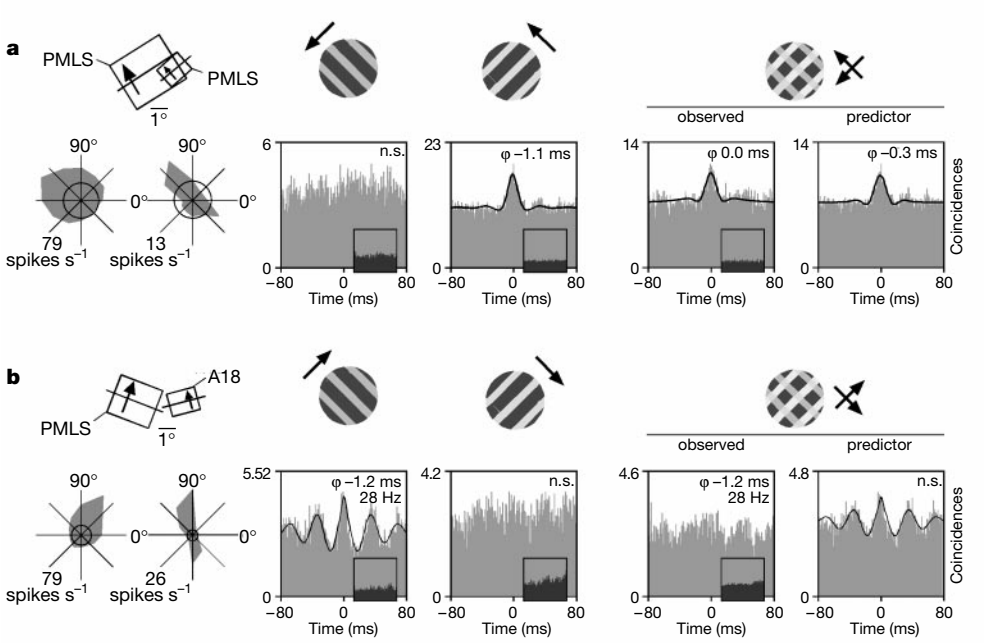

Figure 2 Comparison between single gratings and plaids. **a**, Synchronization between neurons with similar direction preferences and colinearly arranged, spatially contiguous RFs recorded from area PMLS. Correlograms are from responses to single gratings moving in the cells' non-preferred (first) and preferred direction (second) and from responses to a transparent plaid resulting from a superposition of the two gratings (third correlogram). The fourth correlogram corresponds to the linear predictor. **b**, Same analysis as in **a** for neurons with spatially segregated RFs and differing direction preferences recorded from areas A18 and PMLS. Conventions as in Fig. 1.

remained high and unchanged during the first half of the duty cycle change and then dropped abruptly below the level of significance. By contrast, responses of cells with colinearly aligned, overlapping RFs remained synchronized throughout the change in duty cycle (Fig. 3d).

Classifying cells as component or pattern selective (see Methods and refs 13–16) confirmed that most cells in areas A18 and PMLS of cat visual cortex are best described as component selective (Fig. 4 top and refs 14–16). Furthermore, classification of cells into component- and pattern-selective subsets changed only little when response profiles were obtained with transparent and non-transparent plaids, respectively, indicating that individual cells do not differentiate between transparent and non-transparent conditions (Fig. 4a). To quantify this result, we subtracted the responses obtained with the two different plaid constellations from each other (component minus pattern condition) and reclassified the cells (Fig. 4, top right). Almost none of the resulting data points had any significant correlation with either of the two predictors. This proves that there is no systematic relation between rate changes of neurons in A18 and PMLS and transparency modifications.

Thus, differential synchronization might be the signal that biases perception towards component or pattern motion. To quantify stimulus-dependent changes in synchrony, we performed a split-plot analysis of variance (ANOVA). Synchronization strength was evaluated for each cell pair for responses evoked with single gratings and for responses evoked with both transparent and non-transparent plaids moving in the direction intermediate to those preferred by the respective cells. In the analysis, we also included a linear predictor of synchrony that corresponds to the correlation strength that one expects for plaids if correlations result simply from the sum of the coincidences in the responses to the respective single gratings. Correlation strength determined for the various conditions (pattern, component, single grating and linear predictor) was then related in a multifactorial analysis to the RF configuration of the analysed cell pairs. The following parameters were considered: RF overlap, colinearity of fields with similar direction preferences and difference between direction preferences. This analysis showed no detectable difference between cell pairs distributed within or across areas A18 and PMLS, so we pooled the data from all cell pairs. As predicted, responses of neuron pairs whose RFs differed in all the chosen categories (position, colinearity and direction preference) exhibit a highly significant reduction in synchrony when plaids undergo modifications that bias perception from pattern to component motion ($P \ll 0.01$, split-plot ANOVA, Fig. 4b). Conversely, no significant changes in synchrony ($P > 0.3$) occurred for cell pairs whose RFs had the same direction preference and were in addition either overlapping or colinear, conditions in which responses are likely to result from the same contour.

To illustrate the dependence of synchrony on both the transparency condition and the direction of plaid motion, we plotted synchronization strength against direction of plaid motion for transparent and non-transparent plaids as well as for a single grating (Fig. 4c). In this analysis we included only cells with strong direction preferences ($n = 25$) but pooled all pairs with similar and differing direction preferences. Differences in synchronization were maximal when plaid motion was in the direction intermediate to those preferred by the respective cells, the 'zero' direction. In this case non-transparent plaids induced strong synchronization whereas transparent plaids caused a complete break down of synchrony. When the direction of movement was offset from 'zero' by more than 30°, when one of the component gratings moved in a direction close to 'zero', differences between transparent and non-transparent conditions were less pronounced, because cells whose direction preference differed by less than 20° synchronized in both conditions. Single gratings induced synchrony at all directions of motion that evoked strong responses at both sites. This indicates that transparent plaids moving in 'zero' direction induce active desynchronization of

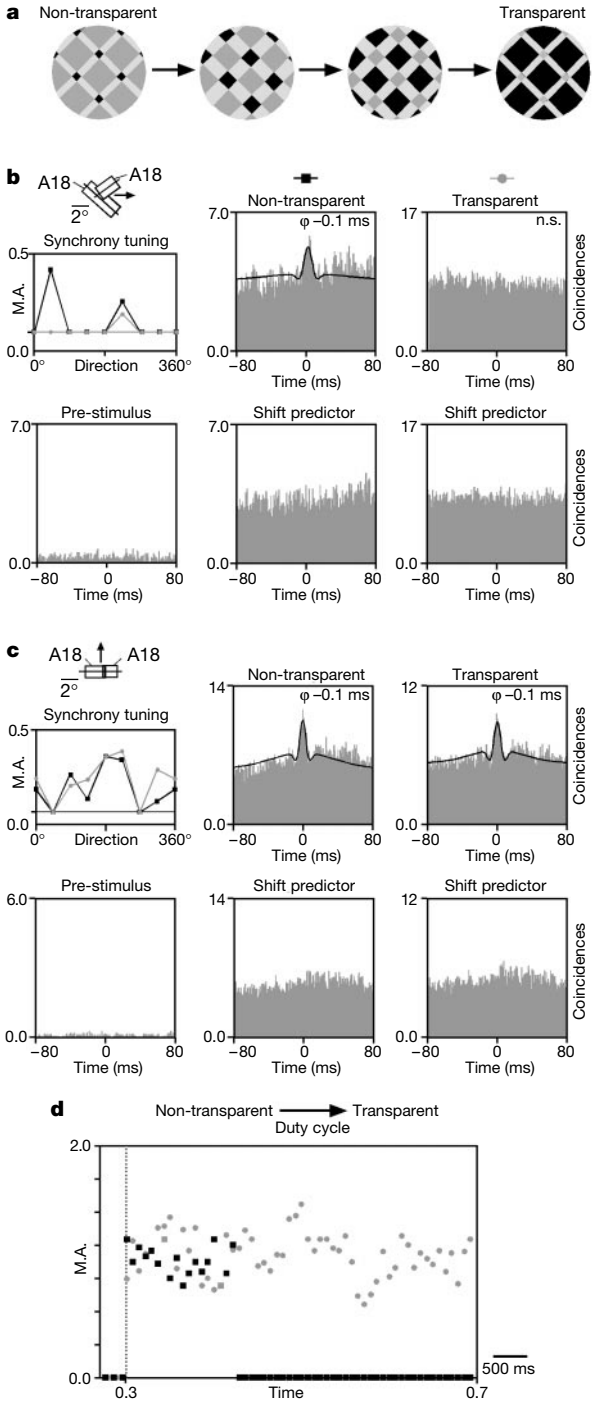

Figure 3 Changes in synchrony induced by manipulating the duty cycle of plaid components. **a**, A progressive change in duty cycle induces a change from non-transparent to transparent motion because of a flip in foreground–background assignment[1,9]. **b**, **c**, Dependence of synchrony on the direction of plaid motion and transparency conditions for two cell pairs in A18 with discordant (**b**) and concordant (**c**) RFs. Left (synchrony tuning), relative modulation amplitude (MA) of correlation peaks for different directions of plaid motion (abscissa: 0°, horizontal right; 90°, vertical up) for non-transparent (dark squares) and transparent (grey circles) plaids. Middle and right, cross-correlograms for responses to non-transparent and transparent plaids moving in a direction intermediate between the cells' preferences (**b**) and in the cells' preferred direction (**c**). Bottom, pre-stimulus correlograms and shift predictors. **d**, Sliding window analysis (step 100 ms, window 400 ms) of changes of correlation strength (ordinate) resulting from duty cycle modifications (between 0.7 and 0.3, abscissa) for the cell pairs shown in **b** (black squares) and **c** (grey circles).

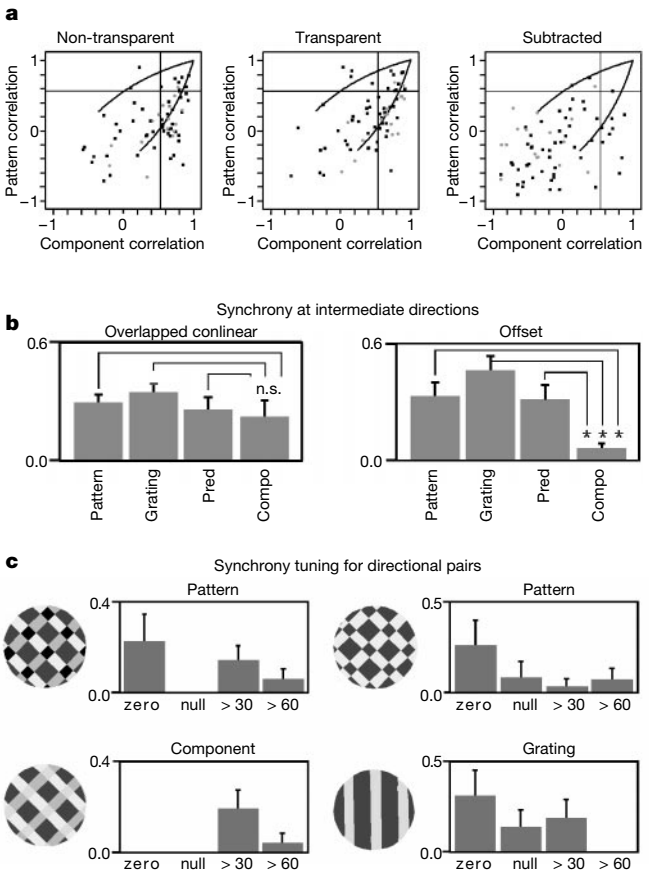

Figure 4 Effect of transparency manipulation on response amplitudes and synchrony. **a**, Scatter plots identifying cells as component (abscissa) or pattern selective (ordinate) obtained from responses to non-transparent (left) and transparent plaids (middle). Continuous lines indicate significance of classification. Cells in upper left and lower right cases are classified as pattern and component selective, respectively. Cells outside these regions or inside the curved area are unclassified. Right, classification after subtraction of responses to non-transparent plaids from those to transparent plaids. Dark squares and grey circles, stimuli in which either the duty cycle (squares) or the luminance of intersections (circles) have been manipulated. **b**, Comparison of correlation strength (ordinate) for non-transparent (pattern) and transparent (component) plaids, single gratings (grating) and the linear predictor (pred) for cell pairs with overlapping, colinear (top) and non-overlapping, dissimilar RFs (bottom). Responses were evoked with plaids (gratings) moving in a direction intermediate to those preferred by the respective cells. **c**, Dependence of correlation strength (ordinate) on stimulus conditions (pattern, component, grating) and direction of stimulus motion (abscissa) for the subset of cells with strong directional preferences ($n = 25$). Zero, stimuli moving in a direction intermediate ($\pm$ 30°) to the cells' preferred directions; null, direction opposite to zero; $>$ 30 and $>$ 60, directions offset by at least 30° or 60° from zero.

cells responding to the respective components.

In early visual areas such as those investigated here, most cells are component specific and, as our data indicate, their rate-modulated responses do not distinguish between pattern and component motion conditions[13–16]. This calls for a transparency-sensitive, rate-independent grouping cue that permits subsequent processing stages to associate responses with either a single or two different surfaces. We propose that the differential synchronization of the responses of component-selective cells described here could serve as the required grouping signal, because synchrony occurred selectively among exactly those responses that need to be bound to account for the different perceptions induced by plaids of different transparency.

For the read-out of these differential synchronization patterns, two non-exclusive possibilities may be considered. Coincidence detectors in higher processing areas could transform the synchronized output of cells in A18 and PMLS in rate codes for the various surfaces in plaid stimuli. Alternatively, the synchronously active ensembles of neurons distributed across areas A18 and PMLS, and presumably also other cortical areas, could themselves serve as the distributed representations of the surfaces. Changes in cortical synchronization patterns are sensed by output structures such as the optic tectum[21] and can thus lead to modification of eye movements without requiring further decoding[22].

In conclusion, the present findings provide evidence that synchronization correlates well with the perceptual segmentation of a complex visual pattern into distinct, spatially overlapping surfaces. As no such correlation was found for the rate-modulated responses of neurons in the cortical areas analysed here, we propose that synchronization serves to group responses for further joint evaluation. □

Methods

Anaesthesia was induced with ketamine (Ketanest, Parke–Davis, 10 mg kg^{-1}, intramuscular) and xylazine (Rompun, Bayer, 2 mg kg^{-1}, intramuscular), and maintained with a mixture of 70% N_2O and 30% O_2 supplemented by 0.5–1.0% halothane. Paralysis was obtained with pancuronium bromide (Pancuronium, Organon, 0.15 mg kg^{-1} h^{-1}). Single- or multi-unit activity (306 recording pairs in six animals) was recorded with multiple (up to four) varnish-coated tungsten electrodes[23]. Cortical areas A18 and PMLS were identified on the basis of RF properties and histology[24]. Signals were band-pass filtered from 1 to 3 kHz and spikes were detected with an amplitude discriminator with the threshold set to twice the noise level.

Visual stimuli were generated on a computer screen (refresh rate of 100 Hz). Squarewave gratings were superimposed in a circular display subtending 12–18° of visual angle. Transparent and non-transparent plaids were interleaved with single gratings and moved in up to twelve different directions, movement direction changing from trial to trial in a pseudorandom sequence (20 trials per configuration).

Plaid velocities (pattern velocity, 8 and 16° s^{-1}), background, grating and intersection luminances (0.5–140 cd m^{-2}, mean stimulus luminance ~35 cd m^{-2}), duty cycle (around 0.3) and angle between gratings (preferably above 135°) were adjusted to induce strong perceptual biases. Stimulus conditions were validated by analysing eye movements from

electro-oculographic recordings in two awake cats and this indicated that the animals distinguished between component and pattern motion.

Auto- and cross-correlograms were calculated for responses from individual trials with a resolution of 1.0 ms and averaged over 20 stimulus presentations. Pre-stimulus correlograms controlled for stimulus independent correlations and shift predictors for synchronization induced by stimulus-locking[25]. A damped cosine function was fitted to the correlograms to quantify the strength and phase shift of correlations and the frequency and modulation depth of oscillatory patterning[23,26]. Correlation strength was assessed from the modulation amplitude (MA), the ratio between the amplitude of the central peak of both the fitted and the raw function (as a control) and the correlogram offset. MA values obtained with and without normalization to the geometric mean of firing rates (normalized coincidences) gave similar results.

A split-plot design[27] was applied (ANOVA for repeated measures) to evaluate correlation strength as a function of stimulus (pattern and component motion, single gratings, linear predictor derived from responses to single gratings) and RF configuration. Orientation and direction preferences, and tuning width were determined with vector averaging methods[28,29]. Recording sites were classified as having similar orientation preferences if these differed by less than 20°, as having colinear RFs if the offset of the axial alignment of the RFs was $<$ 20% of the size of the smaller RF, and as having overlapping RFs if discharge regions (mapped with small moving bars) overlapped. RFs were classified as directional if the ratio of responses to stimuli in preferred and non-preferred directions was $\geqslant 2$ (true for 106 pairs). 55 pairs differed and 16 pairs matched in all categories; 25 pairs exhibited strong directional tuning at both sites.

Based on firing rate, neurons were classified as component selective if the directional tuning curve obtained with plaids correlated with that resulting from linear summation of the responses to the respective component gratings. Conversely, cells were classified as pattern-selective if the tuning curve obtained with a plaid correlated better with that resulting from stimulation with a single grating. Computation of statistical boundaries took into account the number of stimulus directions and the number of stimulus trials. The partial correlations were computed with the following equation: $R_p = (r_p - r_c r_{pc})/[(1 - r_c^2)(1 - r_{pc}^2)]^{1/2}$. R_p, partial correlation coefficient for the pattern prediction; r_c, correlation coefficient between the plaid response and the component model; r_p, correlation coefficient between the plaid response and the pattern model; r_{pc}, correlation coefficient for the two models. Also R_c is the partial correlation coefficient for the component prediction, obtained by interchanging r_p and r_c[13].

Received 24 January; accepted 11 April 2000.

1. Stoner, G. R. & Albright, T. D. The interpretation of visual motion: evidence for surface segmentation mechanisms. *Vision Res.* **36,** 1291–1310 (1996).
2. Shimojo, S., Silverman, G. H. & Nakayama, K. An occlusion-related mechanism of depth perception based on motion and interocular sequence. *Nature* **333,** 265–268 (1988)
3. Movshon, J. A, Adelson, E. H., Gizzi, M. & Newsome, W. T. in *Study Group on Pattern Recognition Mechanisms* (eds Chagas, C. Gatass, R. & Gross, C. G.) (Pontifica Academia Scientiarum, Vatican City, 1985).
4. Adelson, E. H. & Movshon, J. A. Phenomenal coherence of moving visual patterns. *Nature* **300,** 523–525 (1982).
5. Stoner, G. R., Albright, T. D. & Ramachandran, V. S. Transparency and coherence in human motion perception. *Nature* **344,** 153–155 (1990)
6. Smith, A. T. & Harris, L. R. Use of plaid patterns to distinguish the corticofugal and direct retinal inputs to the brainstem optokinetic nystagmus generator. *Exp. Brain Res.* **86,** 324–332 (1991).
7. Metelli, F. The perception of transparency. *Sci. Am.* **230,** 90–98 (1974).
8. Beck, J. & Ivry, R. On the role of figural organization in perceptual transparency. *Percept. Psychophys.* **44,** 585–594 (1988).
9. Albright, T. D. & Stoner, G. R. Visual motion perception. *Proc. Natl Acad. Sci. USA* **92,** 2433–2440 (1995).
10. Stoner, G. R. & Albright T. D. Luminance contrast affects motion coherency in plaid patterns by acting as depth from occlusion cue. *Vision Res.* **38,** 387–401 (1998).
11. Stoner, G. R. & Albright, T. D. Neural correlates of perceptual motion coherence. *Nature* **358,** 412–414 (1992).
12. Castelo-Branco, M. *et al.* MT/MST activation depends on the interpretation of stimuli: a functional fMRI study of the perception of plaids. *Soc. Neurosci. Abstr.* **23,** 460 (1997).
13. Rodman, H. R. & Albright, T. D. Single-unit analysis of pattern-motion selective properties in the middle temporal visual area (MT). *Exp. Brain Res.* **75,** 53–64 (1989).
14. Gizzi, M. S., Katz, E., Schumer, R. A. & Movshon, J. A. Selectivity for orientation and direction of motion of single neurons in cat striate and extrastriate visual cortex. *J. Neurophysiol.* **63,** 1529–1543 (1990).
15. Scannell, J. W. *et al.* Visual motion processing in the anterior ectosylvian sulcus of the cat. *J. Neurophysiol.* **76,** 895–907 (1996).
16. Merabet, L., Desautels, A., Minville, K. & Casanova, C. Motion integration in a thalamic visual nucleus. *Nature* **396,** 265–268 (1998).
17. Gray, C. M., Konig, P., Engel, A. K. & Singer, W. Oscillatory responses in cat visual cortex exhibit inter-columnar synchronization which reflects global stimulus properties. *Nature* **338,** 334–337 (1989).
18. Engel, A. K., Konig, P., Kreiter, A. K. & Singer, W. Interhemispheric synchronization of oscillatory neuronal responses in cat visual cortex. *Science* **252,** 1177–1179 (1991).
19. Freiwald, W. A., Kreiter, A. K. & Singer, W. Stimulus dependent intercolumnar synchronization of single unit responses in cat area 17. *NeuroReport* **6,** 2348–2352 (1995).
20. Kreiter, A. K. & Singer, W. Stimulus-dependent synchronization of neuronal responses in the visual cortex of the awake macaque monkey. *J. Neurosci.* **16,** 2381–2396 (1996).
21. Brecht, M., Singer, W. & Engel, A. K. Correlation analysis of corticotectal interactions in the cat visual system. *J. Neurophysiol.* **79,** 2394–2407 (1998).
22. Brecht, M., Singer, W. & Engel, A. K. Collicular saccade vectors defined by synchronization. *Soc. Neurosci. Abstr.* **23,** 843 (1997).
23. Castelo-Branco, M., Neuenschwander, S. & Singer, W. Synchronization of visual responses between the cortex, lateral geniculate nucleus, and retina in the anesthetized cat. *J. Neurosci.* **18,** 6395–6410 (1998).
24. Palmer, L. A., Rosenquist, A. C. & Tusa, R. J. The retinotopic organization of lateral suprasylvian visual areas in the cat. *J. Comp. Neurol.* **177,** 237–256 (1978).
25. Perkel, D. H., Gerstein, G. L. & Moore, G. P. Neuronal spike trains and stochastic point processes. II. Simultaneous spike trains. *Biophys. J.* **7,** 419–440 (1967).
26. König, P. A method for the quantification of synchrony and oscillatory properties of neuronal activity. *J. Neurosci. Methods* **54,** 31–37 (1994).
27. Edwards, A. L. *Multiple Regression Analysis and the Analysis of Variance and Covariance* (W. H. Freeman, New York, 1985).
28. Batschelet, E. *Circular Statistics in Biology* (Academic, London, 1993).
29. Swindale, N. V. Orientation tuning curves: empirical description and estimation of parameters. *Biol. Cybern.* **78,** 45–56 (1998).

Acknowledgements

We thank H. Klon-Lipok, P. Janson and S. Grimm for their technical assistance in electrode manufacture and histology. This research was sponsored by the Max-Planck-Gesellschaft. M.C.-B. was partially supported by the Gulbenkian Foundation and Programa Praxis, Portugal.

Correspondence and requests for materials should be addressed to: W.S. (e-mail: singer@mpih-frankfurt.mpg.de).

Photoactivated γ-secretase inhibitors directed to the active site covalently label presenilin 1

Yue-Ming Li*, Min Xu*, Ming-Tain Lai*, Qian Huang*, José L. Castro†, Jillian DiMuzio-Mower*, Timothy Harrison†, Colin Lellis*, Alan Nadin†, Joseph G. Neduvelil†, R. Bruce Register*, Mohinder K. Sardana*, Mark S. Shearman†, Adrian L. Smith†, Xiao-Ping Shi*, Kuo-Chang Yin*, Jules A. Shafer* & Stephen J. Gardell*

** Department of Biological Chemistry, Merck Research Laboratories, West Point, Pennsylvania 19486, USA*
† Neuroscience Research Centre, Merck Sharp & Dohme Research Laboratories, Terlings Park, Harlow, Essex CM20 2QR, UK

Cleavage of amyloid precursor protein (APP) by the β- and γ-secretases generates the amino and carboxy termini, respectively, of the Aβ amyloidogenic peptides Aβ40 and Aβ42—the major constituents of the amyloid plaques in the brain parenchyma of Alzheimer's disease patients[1]. There is evidence that the polytopic membrane-spanning proteins, presenilin 1 and 2 (PS1 and PS2), are important determinants of γ-secretase activity: mutations in PS1 and PS2 that are associated with early-onset familial Alzheimer's disease[2,3] increase the production of Aβ42 (refs 4–6), the more amyloidogenic peptide; γ-secretase activity is reduced in neuronal cultures derived from PS1-deficient mouse embryos[7]; and directed mutagenesis of two conserved aspartates in transmembrane segments of PS1 inactivates the ability of γ-secretase to catalyse processing of APP within its transmembrane domain[8]. It is unknown, however, whether PS1 (which has little or no homology to any known aspartyl protease) is itself a transmembrane aspartyl protease or a γ-secretase cofactor, or helps to colocalize γ-secretase and APP. Here we report photoaffinity labelling of PS1 (and PS2) by potent γ-secretase inhibitors that were designed to function as transition state analogue inhibitors directed to the active site of an aspartyl protease. This observation indicates that PS1 (and PS2) may contain the active site of γ-secretase. Interestingly, the intact, single-chain form of wild-type PS1 is not labelled by an active-site-directed photoaffinity probe, suggesting that intact wild-type PS1 may be an aspartyl protease zymogen.

We used L-685,458 (Fig. 1), a potent γ-secretase inhibitor[9], to prepare photoaffinity probes that label the active site of γ-secretase.

tri-NaCitrate and 20% PEG 3350, at a final pH of 7.4 (PEG/Ion Screen, Hampton Research, San Diego, California) within two weeks at 4 °C. Intact complex was verified by SDS–polyacrylamide gel electrophoresis of washed crystals (see Supplementary Information). Data were collected from a single frozen crystal, cryoprotected in 28.5% PEG 4000 and 10% PEG 400, at beamline 9.6 at the SRS Daresbury, UK.

The data were processed using MOSFLM[24] and merged using SCALA[25] from the CCP4 package[26] (Table 1) The molecular replacement solution for α_1-antitrypsin in the complex was obtained using AMORE[27] and the structure of cleaved α_1-antitrypsin[28] as the search model. Conventional molecular replacement searches failed to place a model of intact trypsin[29] in the complex, although maps calculated with phases from α_1-antitrypsin alone showed clear density for the ordered portion of trypsin (Fig. 3 and Supplementary Information). It was immediately apparent that density was only present for about half of the volume expected to be occupied by intact trypsin. A search model comprising trypsin residues 27–124 and 230–245 was orientated using AMORE to compute a domain rotation function[30] against structure factors corresponding to a sphere of the ordered density, which were calculated using the program GHKL (L. Tong, unpublished data). The position of the oriented model relative to α_1-antitrypsin was determined with AMORE using the original diffraction data. The entire model of trypsin was superimposed on the fragment and then truncated to the limits of the electron density to provide an initial model of the complex. The truncated model, to our surprise, was nearly complete in accounting for the ordered structure contributing to the diffraction data, despite including only about 50% of the trypsin residues. In fact, the amount of ordered density changed little throughout the course of refinement. Completeness of this model was estimated at 99% by a σ_A-plot computed in the program SIGMAA[31]. The model comprising α_1-antitrypsin alone was estimated to be 83% complete, whereas α_1-antitrypsin comprises only 62% of the mass of the complex (σ_A-plots are included as Supplementary Information). The final molecular model was achieved through an iterative procedure of rebuilding using XtalView and refinement in CNS[32] using a maximum likelihood target[33]. Statistics for data processing, refinement and for the final model are given in Table 1. Figures were made using the programs Molscript[34], Bobscript[35] and Raster3D[36].

Received 10 May; accepted 2 August 2000.

1. Potempa, J., Korzus, E. & Travis, J. The serpin superfamily of proteinase inhibitors: structure, function, and regulation. *J. Biol. Chem.* **269,** 15957–15960 (1994).
2. Laskowski, M. & Qasim, M. A. What can the structures of enzyme-inhibitor complexes tell us about the structures of enzyme substrate complexes? *Biochim. Biophys. Acta* **1477,** 324–337 (2000).
3. Loebermann, H., Tokuoka, R., Deisenhofer, J. & Huber, R. Human alpha 1-proteinase inhibitor. Crystal structure analysis of two crystal modifications, molecular model and preliminary analysis of the implications for function. *J. Mol. Biol.* **177,** 531–557 (1984).
4. Huber, R. & Bode, W. Structural basis of the activation and action of trypsin. *Acc. Chem. Res.* **11,** 114–122 (1978).
5. Kaslik, G., Patthy, A., Balint, M. & Graf, L. Trypsin complexed with alpha 1-proteinase inhibitor has an increased structural flexibility. *FEBS Lett.* **370,** 179–183 (1995).
6. Stavridi, E. S. *et al.* Structural change in alpha-chymotrypsin induced by complexation with alpha 1-antichymotrypsin as seen by enhanced sensitivity to proteolysis. *Biochemistry* **35,** 10608–10615 (1996).
7. Huber, R. & Carrell, R. W. Implications of the three-dimensional structure of alpha 1-antitrypsin for structure and function of serpins. *Biochemistry* **28,** 8951–8966 (1989).
8. Elliott, P. R., Abrahams, J. P. & Lomas, D. A. Wild-type alpha 1-antitrypsin is in the canonical inhibitory conformation. *J. Mol. Biol.* **275,** 419–425 (1998).
9. Wright, H. T. & Scarsdale, J. N. Structural basis for serpin inhibitor activity. *Proteins* **22,** 210–225 (1995).
10. Stratikos, E. & Gettins, P. G. Formation of the covalent serpin–proteinase complex involves translocation of the proteinase by more than 70 A and full insertion of the reactive center loop into beta-sheet A. *Proc. Natl Acad. Sci. USA* **96,** 4808–4813 (1999).
11. Fa, M. *et al.* The structure of a serpin-proteinase complex revealed by intramolecular distance measurements using donor-donor energy migration and mapping of interaction sites. *Structure* **8,** 397–405 (2000).
12. Picard, V., Marque, P. E., Paolucci, F., Aiach, M. & Le Bonniec, B. F. Topology of the stable serpin–protease complexes revealed by an autoantibody that fails to react with the monomeric conformers of antithrombin. *J. Biol. Chem.* **274,** 4586–4593 (1999).
13. Carrell, R. W. & Owen, M. C. Plakalbumin, alpha 1-antitrypsin, antithrombin and the mechanism of inflammatory thrombosis. *Nature* **317,** 730–732 (1985).
14. Stein, P. E. *et al.* Crystal structure of ovalbumin as a model for the reactive centre of serpins. *Nature* **347,** 99–102 (1990).
15. Engh, R. A., Huber, R., Bode, W. & Schulze, A. J. Divining the serpin inhibition mechanism: a suicide substrate 'spring'? *Trends Biotechnol.* **13,** 503–510 (1995).
16. Gooptu, B. *et al.* Inactive conformation of the serpin alpha(1)-antichymotrypsin indicates two-stage insertion of the reactive loop: implications for inhibitory function and conformational disease. *Proc. Natl Acad. Sci. USA* **97,** 67–72 (2000).
17. Herve, M. & Ghelis, C. Conformational stability of the covalent complex between elastase and alpha 1-proteinase inhibitor. *Arch. Biochem. Biophys.* **285,** 142–146 (1991).
18. Olson, S. T. *et al.* Role of the catalytic serine in the interactions of serine proteinases with protein inhibitors of the serpin family. Contribution of a covalent interaction to the binding energy of serpin–proteinase complexes. *J. Biol. Chem.* **270,** 30007–30017 (1995).
19. Plotnick, M. I., Mayne, L., Schechter, N. M. & Rubin, H. Distortion of the active site of chymotrypsin complexed with a serpin. *Biochemistry* **35,** 7586–7590 (1996).
20. Gils, A. & Declerck, P. J. Structure-function relationships in serpins: current concepts and controversies. *Thromb. Haemost.* **80,** 531–541 (1998).
21. Harrop, S. J. *et al.* The crystal structure of plasminogen activator inhibitor 2 at 2. 0 Å resolution: implications for serpin function. *Struct. Fold Des.* **7,** 43–54 (1999).
22. Holmes, W. E. *et al.* Alpha 2-antiplasmin Enschede: alanine insertion and abolition of plasmin inhibitory activity. *Science* **238,** 209–211 (1987).
23. Bode, W. & Huber, R. Structural basis of the endoproteinase-protein inhibitor interaction. *Biochim. Biophys. Acta* **1477,** 241–252 (2000).
24. Leslie A. W. G. in *Joint CCP4 and ESF-EACMB Newsletter on Protein Crystallography* vol. 26 (Daresbury Laboratory, Warrington, 1992).
25. Evans P. R. in *Proceedings of the CCP4 Study Weekend. Data Collection and Processing* (eds Sawyer, L., Isaacs, N. & Bailey, S.) 114–122 (Daresbury Laboratory, 1993).
26. Collaborative Computational Project Number 4. The CCP4 suite: programs for protein crystallography. *Acta Crystallogr.* **50,** 760–763 (1994).
27. Navaza, J. AMORE - An automated package for molecular replacement. *Acta Cryst. A* **50,** 157–163 (1994).
28. Engh, R. *et al.* The S variant of human alpha 1-antitrypsin, structure and implications for function and metabolism. *Protein Eng.* **2,** 407–415 (1989).
29. Lee, S. L. New inhibitors of thrombin and other trypsin-like proteases: hydrogen bonding of an aromatic cyano group with a backbone amide of the P1 binding site replaces binding of a basic side chain. *Biochemistry* **36,** 13180–13186 (1997).
30. Colman, P. M., Fehlhammer, H. & Bartles, K. in *Crystallographic Computing Techniques* (eds Ahmed, F. R., Huml, K. & Sedlacek, B.) 248–258 (Munksgaard, Copenhagen, 1976).
31. Read, R. J. Improved Fourier coefficients for maps using phases from partial structures with errors. *Acta Cryst. A* **42,** 140–149 (1986).
32. Brunger, A. T. *et al.* Crystallography & NMR system: A new software suite for macromolecular structure determination. *Acta Cryst. D* **54,** 905–921 (1998).
33. Pannu, N. S. & Read, R. J. Improved structure refinement through maximum likelihood. *Acta Cryst. A* **52,** 659–668 (1996).
34. Kraulis, P. J. MOLSCRIPT: a program to produce both detailed and schematic plots of protein structures. *J. Appl. Crystallogr.* **24,** 946–950 (1991).
35. Esnouf, R. Further additions to MolScript version 1.4, including reading and contouring of electron-density maps. *Acta Crystallogr. D* **55,** 938–940 (1999).
36. Merritt, E. A. & Bacon, D. J. Raster3D: photorealistic molecular graphics. *Methods Enzymol.* **277,** 505–524 (1997).

Supplementary information is available on *Nature*'s World-Wide Web site (http://www.nature.com) or as paper copy from the London editorial office of *Nature*.

Acknowledgements

We thank our colleagues, N. Pannu for advice throughout; D. Lomas for reading the paper; A. Lesk and P. Stein for discussions; and K. Belzar for support. This work was supported by grants from the Wellcome Trust, the European Community and the National Institutes of Health (J.A.H.).

Correspondence and requests for materials should be addressed to J.A.H. (e-mail: jah52@cam.ac.uk) or R.W.C. (e-mail: rwc1000@cam.ac.uk). Atomic coordinates have been deposited in the Protein Data Bank under accession code 1EZX.

errata

Intraprotein radical transfer during photoactivation of DNA photolyase

Corrine Aubert, Marten H. Vos, Paul Mathis, André P. M. Eker & Klaus Brettel

Nature **405,** 586–590 (2000).

Figure 5 of this paper contained an error. The lower right-hand box in the reaction scheme, which read 'FADH$^-$ TrpH TrpH TrpH$^{\bullet}$', should have read 'FADH$^-$ TrpH TrpH Trp$^{\bullet}$'. □

Neural synchrony correlates with surface segregation rules

Miguel Castelo-Branco, Rainer Goebel, Sergio Neuenschwander & Wolf Singer

Nature **405,** 685–689 (2000).

In Fig. 1b of this Letter, the scale bar for the repetitive fields should be half as large as it was printed. In Fig. 1c, the label that reads PMLS should read A18. □